Electric Power Systems Research 97 (2013) 51–60

Contents lists available at SciVerse ScienceDirect

Electric Power Systems Research

journal homepage: www.elsevier.com/locate/epsr

A mixed-integer LP model for the reconfiguration of radial electric distribution systems considering distributed generation

John F. Franco, Marcos J. Rider*, Marina Lavorato, Rubén Romero

Universidade Estadual Paulista (UNESP), Faculdade de Engenharia de Ilha Solteira (FEIS), Departamento de Engenharia Elétrica (DEE), Ilha Solteira, São Paulo, Brazil

ARTICLE INFO

Article history:
Received 19 July 2012
Received in revised form
30 September 2012
Accepted 10 December 2012
Available online 16 January 2013

Keywords:
Reconfiguration of electric distribution systems
Active power losses reduction
Distributed generation
Mixed-integer linear programming

ABSTRACT

The problem of reconfiguration of distribution systems considering the presence of distributed generation is modeled as a mixed-integer linear programming (MILP) problem in this paper. The demands of the electric distribution system are modeled through linear approximations in terms of real and imaginary parts of the voltage, taking into account typical operating conditions of the electric distribution system. The use of an MILP formulation has the following benefits: (a) a robust mathematical model that is equivalent to the mixed-integer non-linear programming model; (b) an efficient computational behavior with exiting MILP solvers; and (c) guarantees convergence to optimality using classical optimization techniques. Results from one test system and two real systems show the excellent performance of the proposed methodology compared with conventional methods.

1. Introduction

The reconfiguration of the distribution system (RDS) is one of the classic optimization problems in the operation of electrical distribution systems (EDS). In addressing this problem, the main objective is to find the best radial topology in order to obtain minimum active power losses, meet the energy demand, and maintain system reliability. This procedure can permit an efficient and reliable operation. Due to various technical reasons, the EDS must operate with a radial topology (even though it has a mesh structure), the two most important factors being: (a) facilitation coordination and protection; and (b) achieving a reduction of short-circuit current in EDS. The RDS is a problem related to the operation planning of EDS and can be modeled as a highly complex mixed-integer nonlinear programming (MINLP) problem [1].

Some works presented in the specialized literature propose mixed-integer linear and quadratic programming models for the RDS problem. In [2], the authors present a linear model for the RDS problem using the so-called transportation method and a comparison with heuristics methods is made. In [3], the RDS problem is formulated as a minimum cost network flow problem and is solved using a modified simplex method, ignoring the branch capacity limits. In [4], the authors extend the method in [3] with the presence of distributed generation. In [5], two methodologies are used to solve the RDS problem. The first methodology models the RDS problem as a mixed-integer linear programming problem (due to the linearization of the objective function and constraints) and solves it using a standard optimization package. In the second technique, the same problem is modeled as a mixed-integer nonlinear problem and is solved by means of a genetic algorithm. The paper concludes that the results of both methodologies are similar for the tests completed. An extension from [5] is presented in [6], in which the RDS problem is modeled as a mixed-integer quadratic programming problem. A mixed-integer conic programming formulation for the RDS problem is shown in [7].

Several optimization techniques have been offered in the literature to solve the RDS problem. These techniques can be separated into two major groups: (1) exact techniques and (2) heuristic and metaheuristic techniques. The exact techniques, such as branch and bound algorithms, were used only for relaxed models [1,5,6]. However, more recently, heuristics and metaheuristics have been successfully applied with complete models. Simulated annealing [8,9], ant colony [10,11], particle swarm optimization [12], genetic algorithm [13–15] and tabu search algorithms (TSA) [16,17] are among the metaheuristic techniques used to solve the RDS problem. Constructive heuristic algorithms, as seen in [18–22], are among the heuristic algorithms used to solve the RDS problem.

In this paper, the problem of reconfiguration of electric distribution systems considering the presence of distributed generation is modeled as a mixed-integer linear programming (MILP) problem. Linearizations were made to represent adequately the steady-state operation of the EDS considering the behavior of the constant

* Corresponding author at: UNESP – FEIS – DEE, Av. Brasil 56, Centro, CEP: 15385-000, Ilha Solteira, São Paulo, Brazil.
E-mail addresses: johnfranco@dee.feis.unesp.br (J.F. Franco), mjrider@dee.feis.unesp.br (M.J. Rider), marina@dee.feis.unesp.br (M. Lavorato), ruben@dee.feis.unesp.br (R. Romero).

0378-7796/$ – see front matter.
http://dx.doi.org/10.1016/j.epsr.2012.12.005

power type load. The integer nature of the decision variables represents the state of the branches that can be opened or closed in the EDS. The objective is to minimize the active power losses subject to operational and physical constraints. The proposed model was tested using one test system of 69 nodes and two real systems of 136 and 417 nodes. In order to validate the approximations performed, a steady-state operation point was compared with that obtained using the single phase load flow sweep method.

The main contributions of this paper are as follows:

1. A novel model for the steady-state operation of a EDS through the use of linear expressions.
2. A novel MINLP model for the RDS problem where the radiality constraints are properly considered in the mathematical model. Additionally, an extension of this model considering the distributed generation (DG) operation is presented.
3. A MILP formulation for the RDS problem considering DG has the following benefits: (a) a robust mathematical model that is equivalent to the MINLP model; (b) an efficient computational behavior with exiting MILP solvers; and (c) guarantees convergence to optimality using classical optimization techniques.

2. A mixed-integer nonlinear model for the problem of reconfiguration of EDS

In order to model the problem of reconfiguration of EDS, the following assumptions are made:

1. The loads of EDS are modeled as constant power, constant current and constant impedance types.
2. The steady-state operation of EDS is represented in terms of the real and imaginary parts of the voltage and current flow.
3. The three phase EDS is considered symmetrical and then modeled through their positive sequence network.

The RDS problem can be modeled as a mixed-integer nonlinear programming problem as shown in (1)–(17).

$$\min v = \sum_{ij\in\Omega_l}\left[\left(I_{ij}^{re+}+I_{ij}^{re-}\right)^2+\left(I_{ij}^{im+}+I_{ij}^{im-}\right)^2\right]R_{ij} \tag{1}$$

subject to

$$\sum_{ki\in\Omega_l}\left(I_{ki}^{re+}-I_{ki}^{re-}\right)-\sum_{ij\in\Omega_l}\left(I_{ij}^{re+}-I_{ij}^{re-}\right)+I_{Gi}^{re}=I_{Di}^{re}\quad\forall i\in\Omega_b \tag{2}$$

$$\sum_{ki\in\Omega_l}\left(I_{ki}^{im+}-I_{ki}^{im-}\right)-\sum_{ij\in\Omega_l}\left(I_{ij}^{im+}-I_{ij}^{im-}\right)+I_{Gi}^{im}=I_{Di}^{im}\quad\forall i\in\Omega_b \tag{3}$$

$$V_i^{re}-V_j^{re}+w_{ij}^{re}=R_{ij}(I_{ij}^{re+}-I_{ij}^{re-})-X_{ij}(I_{ij}^{im+}-I_{ij}^{im-})\quad\forall ij\in\Omega_l \tag{4}$$

$$V_i^{im}-V_j^{im}+w_{ij}^{im}=X_{ij}(I_{ij}^{re+}-I_{ij}^{re-})+R_{ij}(I_{ij}^{im+}-I_{ij}^{im-})\quad\forall ij\in\Omega_l \tag{5}$$

$$I_{Di}^{re}=\frac{P_{Di}V_i^{re}+Q_{Di}V_i^{im}}{V_i^{re\,2}+V_i^{im\,2}}\quad\forall i\in\Omega_b \tag{6}$$

$$I_{Di}^{im}=\frac{P_{Di}V_i^{im}-Q_{Di}V_i^{re}}{V_i^{re\,2}+V_i^{im\,2}}\quad\forall i\in\Omega_b \tag{7}$$

$$(I_{ij}^{re+}+I_{ij}^{re-})^2+(I_{ij}^{im+}+I_{ij}^{im-})^2\le\bar{I}_{ij}^2(y_{ij}^+ +y_{ij}^-)\quad\forall ij\in\Omega_l \tag{8}$$

$$\underline{V}^2\le V_i^{re2}+V_i^{im2}\le\overline{V}^2\quad\forall i\in\Omega_b \tag{9}$$

$$|w_{ij}^{re}|\le\overline{w}_{ij}^{re}(1-y_{ij}^+-y_{ij}^-)\quad\forall ij\in\Omega_l \tag{10}$$

$$|w_{ij}^{im}|\le\overline{w}_{ij}^{im}(1-y_{ij}^+-y_{ij}^-)\quad\forall ij\in\Omega_l \tag{11}$$

$$0\le I_{ij}^{re+}\le\bar{I}_{ij}y_{ij}^+\quad\forall ij\in\Omega_l \tag{12}$$

$$0\le I_{ij}^{re-}\le\bar{I}_{ij}y_{ij}^-\quad\forall ij\in\Omega_l \tag{13}$$

$$y_{ij}^+ +y_{ij}^-\le 1\quad\forall ij\in\Omega_l \tag{14}$$

$$\sum_{ij\in\Omega_l}(y_{ij}^+ +y_{ij}^-)=|\Omega_b|-1 \tag{15}$$

$$I_{ij}^{im+},I_{ij}^{im-}\ge 0\quad\forall ij\in\Omega_l \tag{16}$$

$$y_{ij}^+,y_{ij}^-\in\{0,1\}\quad\forall ij\in\Omega_l \tag{17}$$

The objective function of the RDS problem is the minimization of the active power losses of an EDS, as shown in (1). Note that the real part of the current flow of branch ij is represented by two positive variables I_{ij}^{re+} and I_{ij}^{re-}, according to the direction of the current flow; similarly, variables I_{ij}^{im+} and I_{ij}^{im-} are used for the imaginary part of the current flow for branch ij. Constraints (2) and (3) represent respectively the balance of real and imaginary parts of the nodal current at node i (see Fig. 1). Constraints (4) and (5) represent, respectively, the real and imaginary parts of the voltage drop in branch ij. The real and imaginary parts of the currents demanded by the loads are determined by (6) and (7), where P_{Di} and Q_{Di} varies according to the voltage magnitude at node i, as shown in Appendix A, to represent the loads as constant power, constant current and constant impedance loads. Constraints (8) and (9) represent the current flow capacity of each branch and the limits of the voltage magnitude, respectively.

The state of the branch ij is determined by the binary decision variables y_{ij}^+ and y_{ij}^-. If y_{ij}^+ or y_{ij}^- are equal 1, then the branch ij is in operation and if both y_{ij}^+ and y_{ij}^- are zero then the branch ij is out of operation. Despite the fact that the state of a circuit can be represented using only a binary variable, the use of two binary variables makes it possible to limit the direction of the real part of the current flow in the circuit (one binary variable is associated with the forward direction, while the other is associated with the backward direction), which yields better performance. Constraints (10) and (11) state that auxiliary variables w_{ij}^{re} and w_{ij}^{im} are zero if branch ij is in operation. Constants $\overline{w}_{ij}^{re}$ and $\overline{w}_{ij}^{im}$ must be calculated to give a sufficient degree of freedom for w_{ij}^{re} and w_{ij}^{im} in order to satisfy (4) and (5) where branch ij is out of operation. Constraints (12) and (13) define the direction of the real part of the current flows in function of the binary variables y_{ij}^+ and y_{ij}^-, respectively; and constraint (14) ensures that duplication of current flow directions (forward and backward) is not allowed. Note that if $y_{ij}^+=1$, then $y_{ij}^-=0$, $I_{ij}^{re-}=0$, I_{ij}^{re+} is nonzero and the current flow direction is forward. If $y_{ij}^-=1$, then $y_{ij}^+=0$, $I_{ij}^{re+}=0$, I_{ij}^{re-} is nonzero and the current flow direction is backward. Note that $\bar{I}_{ij}$ in (12) and (13) represents the degree of freedom of the variables I_{ij}^{re+} and I_{ij}^{re-} when $y_{ij}^+=1$ or $y_{ij}^-=1$ respectively.

Constraint (15), combined with (2) and (3), is used to obtain a radial topology for the RDS problem, as shown in [23]. The condition of non-negativity for the variables I_{ij}^{im+} and I_{ij}^{im-} is stated in (16). The binary nature of the decision variables is represented by (17), and a feasible operation solution for the EDS depends on their value. The remaining variables represent the operating state of a feasible solution. For a feasible investment proposal, defined through the specified values of y_{ij}^+ and y_{ij}^-, several feasible operation states are possible. Given that R_{ij} is positive in value, the objective function (1) is a convex quadratic function. Constraints (2)–(5) and (10)–(16) are linear, while (6)–(9) are non-linear. With the aim of using a commercial solver, it is desirable to obtain a linear equivalent for (6)–(9) and for the objective function (1).

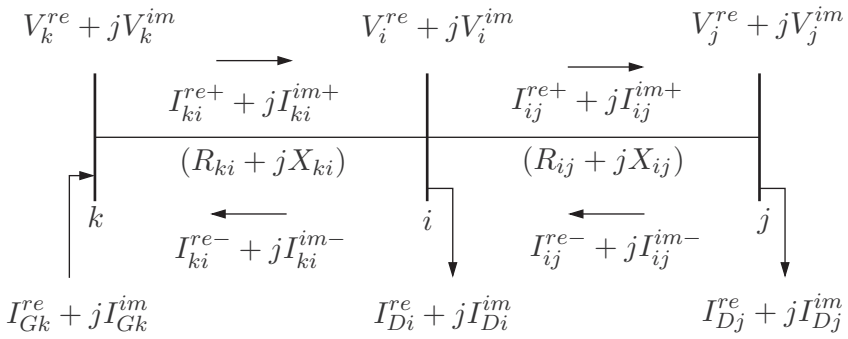

Fig. 1. Illustrative example.

3. Linearization

Note that the real and imaginary parts of the load currents in (6) and (7), the current flow magnitude in (1) and (8) and the voltage magnitude in (9) are non-linear expressions. In this section, these terms will be linearized with the aim of obtaining a mixed-integer linear model for the RDS problem.

3.1. Linearization of the load currents

As seen in Appendix B, the phase angle of the voltage in an EDS has a relatively small and limited range of variation, so we can approximate (6) and (7) by using linear expressions as shown in (18) and (19).

$$I_{Di}^{re} = a_i V_i^{re} + b_i V_i^{im} + c_i \quad \forall i \in \Omega_b \tag{18}$$

$$I_{Di}^{im} = d_i V_i^{re} + e_i V_i^{im} + f_i \quad \forall i \in \Omega_b \tag{19}$$

where a_i, b_i, c_i, d_i, e_i, f_i are coefficients to fit (6) and (7) using (18) and (19) and depend on P_{Di}, Q_{Di} and the variation range of the magnitude and the phase angle of the voltage. These coefficients are calculated for each node i using the least-squares method. For example, for a load of $100 + j60$ kVA at node i, considering a range of [0.9, 1.0] pu for the voltage magnitude (V_i) and $[-5, 2]^\circ$ for the phase angle (θ_i) and using the least-squares method, we obtain the coefficients $a_i = -107.29$, $b_i = 72.13$ and $c_i = 207.22$ for I_{Di}^{re}; and the coefficients $d_i = 72.26$, $e_i = 107.07$ and $f_i = -131.83$ for I_{Di}^{im}. Additionally, the percentual error of the load current magnitude calculated using (18) and (19) and (6) and (7) is shown in Fig. 2. Note that the maximum error is 0.34% and the fitting of (6) and (7) by using (18) and (19) has a correlation coefficient $R^2 = 0.9978$. The high values of R^2 show the very high level of precision of the linearization (18) and (19) used to approximate (6) and (7).

Note that (2)–(5), (18) and (19) are a system of linear equations that represents the steady-state operation of an EDS. This system of linear equations can be used to model other optimization problems of the EDS via linear expressions that can be solved with classical optimization techniques.

3.2. Linearization of the current flow magnitudes

Note that in (1) and (8) appears the square current flow magnitude of branch ij, which can be represented by variable I_{ij}^{sqr} as shown in (20).

$$I_{ij}^{sqr} = (I_{ij}^{re+} + I_{ij}^{re-})^2 + (I_{ij}^{im+} + I_{ij}^{im-})^2 \quad \forall ij \in \Omega_l \tag{20}$$

In (20) there are two quadratic terms and they are linearized using (21) and (22), as shown in Fig. 3.

$$I_{ij}^{sqr} = \sum_{r=1}^{R_{re}} m_{ij,r}^{re} \Delta_{ij,r}^{re} + \sum_{r=1}^{R_{im}} m_{ij,r}^{im} \Delta_{ij,r}^{im} \quad \forall ij \in \Omega_l \tag{21}$$

$$I_{ij}^{re+} + I_{ij}^{re-} = \sum_{r=1}^{R_{re}} \Delta_{ij,r}^{re} \quad \forall ij \in \Omega_l \tag{22a}$$

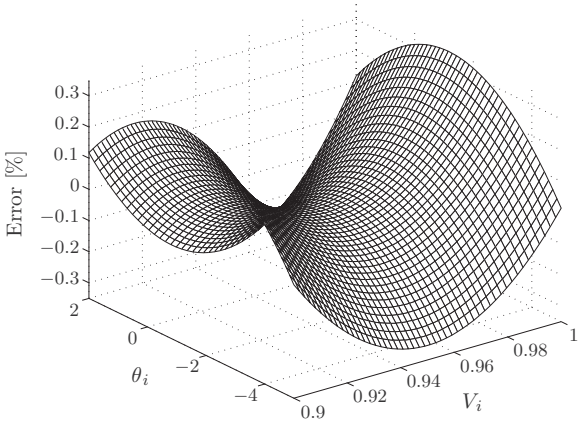

Fig. 2. Current magnitude error.

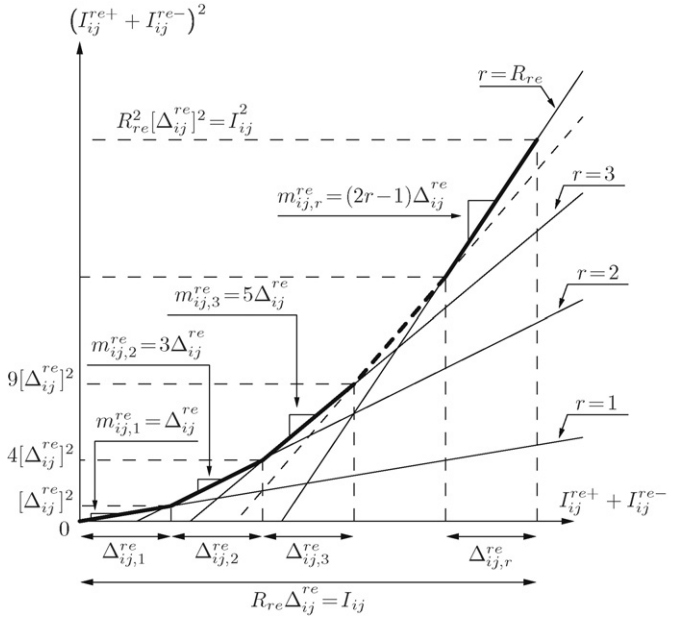

Fig. 3. Modeling the piecewise linear $(I_{ij}^{re+} + I_{ij}^{re-})^2$ function.

$$I_{ij}^{im+} + I_{ij}^{im-} = \sum_{r=1}^{R_{im}} \Delta_{ij,t,r}^{im} \quad \forall ij \in \Omega_l \tag{22b}$$

$$0 \le \Delta_{ij,r}^{re} \le \overline{\Delta}_{ij}^{re} \quad \forall ij \in \Omega_l, r = 1 \ldots R_{re} \tag{22c}$$

$$0 \le \Delta_{ij,r}^{im} \le \overline{\Delta}_{ij}^{im} \quad \forall ij \in \Omega_l, r = 1 \ldots R_{im} \tag{22d}$$

where

$$m_{ij,r}^{re} = (2r-1)\overline{\Delta}_{ij}^{re} \quad \forall ij \in \Omega_l, r = 1 \ldots R_{re}$$

$$\overline{\Delta}_{ij}^{re} = \frac{\bar{I}_{ij}}{R_{re}} \quad \forall ij \in \Omega_l$$

$$m_{ij,r}^{im} = (2r-1)\overline{\Delta}_{ij}^{im} \quad \forall ij \in \Omega_l, r = 1 \ldots R_{im}$$

$$\overline{\Delta}_{ij}^{im} = \frac{\bar{I}_{ij}}{R_{im}} K_{im} \quad \forall ij \in \Omega_l$$

Note that (21) and (22) are a set of linear expressions and $m_{ij,r}^{re}$, $m_{ij,r}^{im}$, $\overline{\Delta}_{ij}^{re}$ and $\overline{\Delta}_{ij}^{im}$ are constant parameters. Constraint (21) is the linear approximation of square current flow magnitude of branch ij, and the terms $\sum_{r=1}^{R_{re}} m_{ij,r}^{re}\Delta_{ij,r}^{re}$ and $\sum_{r=1}^{R_{im}} m_{ij,r}^{im}\Delta_{ij,r}^{im}$ are the linear approximations of $(I_{ij}^{re+} + I_{ij}^{re-})^2$ and $(I_{ij}^{im+} + I_{ij}^{im-})^2$, respectively. Constraints (22a) and (22b) state that $I_{ij}^{re+} + I_{ij}^{re-}$ and $I_{ij}^{im+} + I_{ij}^{im-}$ are equal to the sum of the values in each block of the discretization respectively. Constraints (22c) and (22d) set the upper and lower limits of the contribution of each block of the $I_{ij}^{re+} + I_{ij}^{re-}$ and $I_{ij}^{im+} + I_{ij}^{im-}$ respectively. The K_{im} constant is used to adjust the maximum imaginary current flow as a fraction of current capacity of the branches, taking into account the fact that the imaginary current flows are smaller than the current flow magnitude.

3.3. Linearization of the voltage magnitudes

Because the magnitude and phase angle of the voltages in an EDS have a limited range of variation ($[\underline{V}, \overline{V}]$ and $[\underline{\theta}, \overline{\theta}]$), (9) can be represented by the set of linear constraints (23)–(27), as shown in Fig. 4. Constraints (23)–(27) are related with lines L_1, L_2, L_3, L_4 and L_5 respectively, and limit the voltage magnitudes between $[\underline{V}, \overline{V}]$ and $[\underline{\theta}, \overline{\theta}]$.

$$V_i^{im} \le \frac{\sin\overline{\theta} - \sin\underline{\theta}}{\cos\overline{\theta} - \cos\underline{\theta}}(V_i^{re} - \underline{V}\cos\underline{\theta}) + \underline{V}\sin\underline{\theta} \quad \forall i \in \Omega_b \tag{23}$$

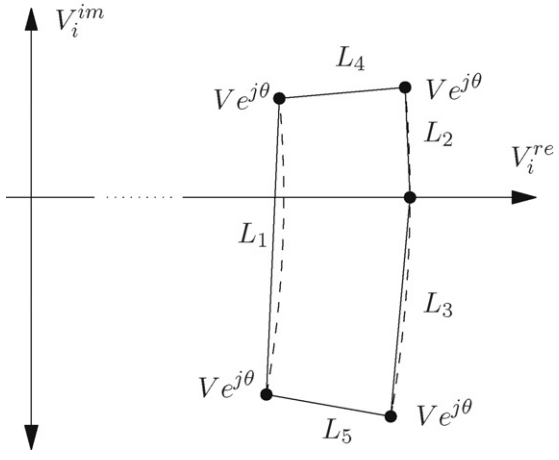

Fig. 4. Constraints for voltage magnitude limits.

$$V_i^{im} \le \frac{\sin\overline{\theta}}{\cos\overline{\theta} - 1}(V_i^{re} - \overline{V}) \quad \forall i \in \Omega_b \tag{24}$$

$$V_i^{im} \le \frac{-\sin\underline{\theta}}{\cos\underline{\theta} - 1}(V_i^{re} - \overline{V}) \quad \forall i \in \Omega_b \tag{25}$$

$$V_i^{im} \le V_i^{re}\tan\overline{\theta} \quad \forall i \in \Omega_b \tag{26}$$

$$V_i^{im} \ge V_i^{re}\tan\underline{\theta} \quad \forall i \in \Omega_b \tag{27}$$

4. A mixed-integer linear model for the problem of reconfiguration of EDS

The RDS problem can be modeled as a mixed-integer linear programming problem as follows:

$$min v = \sum_{ij \in \Omega_l} I_{ij}^{sqr} R_{ij} \tag{28}$$

subject to (2)–(5), (10)–(19) and (21)–(27).

$$I_{ij}^{sqr} \le \bar{I}_{ij}^2 (y_{ij}^{+} + y_{ij}^{-}) \quad \forall ij \in \Omega_l \tag{29}$$

where (28) replaces the objective function (1). Constraints (18) and (19) replace (6) and (7), respectively. Constraints (21), (22) and (29) replace (8). Constraints (23)–(27) replace (9). Note that the number of operation variables has been increased with the linearization, while the number of binary variables does not change and, as will be illustrated later in Section 5, this kind of optimization problem can be solved with the help of standard commercial solvers. The proposed mixed-integer LP model for the RDS problem can be extended to consider the presence of distributed generators in the system.

4.1. Modeling of distributed generation in the problem of reconfiguration of EDS

The operation of a distributed generator can be represented using (30)–(34). It is assumed that the distributed generator has operational limits for the active and reactive supplied power and also for the power factor.

$$P_{Gi} = V_i^{re} I_{Gi}^{re} + V_i^{im} I_{Gi}^{im} \quad \forall i \in \Omega_G \tag{30}$$

$$Q_{Gi} = -V_i^{re} I_{Gi}^{im} + V_i^{im} I_{Gi}^{re} \quad \forall i \in \Omega_G \tag{31}$$

$$0 \le P_{Gi} \le \overline{P}_{Gi} \quad \forall i \in \Omega_G \tag{32}$$

$$\underline{Q}_{Gi} \le Q_{Gi} \le \overline{Q}_{Gi} \quad \forall i \in \Omega_G \tag{33}$$

$$-P_{Gi}\tan(\arccos(pf_{Gi}\downarrow)) \le Q_{Gi} \le P_{Gi}\tan(\arccos(pf_{Gi}\uparrow)) \quad \forall i \in \Omega_G \tag{34}$$

Eqs. (30) and (31) relate the active and reactive power supplied by the distributed generator in terms of the voltage and the real and imaginary parts of the injected current at node i. Constraints (32) and (33) are the active and reactive power limits of the distributed generator respectively, while (34) represents the power factor limits of the distributed generator. Eqs. (30) and (31) are nonlinear and can be linearized using a discretization through binary variables.

The term $V_i^{re} I_{Gi}^{re}$ in (30) is linearized by discretization of V_i^{re} using the binary variables $x_{i,s}^{re}$ $\forall s = 1 \ldots S$, where $x_{i,s}^{re} = 1$ if V_i^{re} is greater than $\underline{V}\cos\beta + s\overline{\zeta}^{re}$ and $\beta = \max\{|\overline{\theta}|, |\underline{\theta}|\}$, as shown in Fig. 5. This condition is modeled in (35), showing how the variables $x_{i,s}^{re}$ are calculated. The constant $\overline{\zeta}^{re}$ establishes the width of each interval

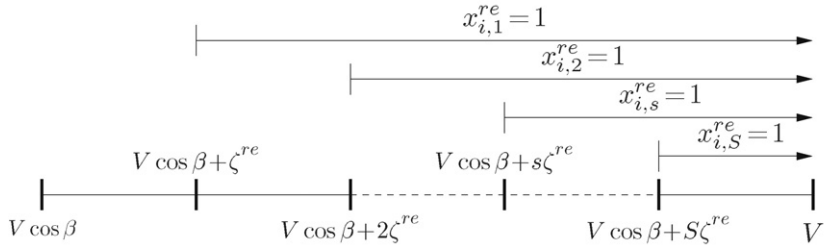

Fig. 5. Discretization of real component of the voltage.

of discretization and it is calculated as $(\overline{V}-\underline{V}\cos\beta)/(S+1)$.

$$\underline{V}\cos\beta+\overline{\zeta}^{re}\sum_{s=1}^{S}x^{re}_{i,s}\le V^{re}_{i}\le\underline{V}\cos\beta+\overline{\zeta}^{re}\left(1+\sum_{s=1}^{S}x^{re}_{i,s}\right)\quad\forall i\in\Omega_G \tag{35a}$$

$$x^{re}_{i,s}\le x^{re}_{i,s-1}\quad\forall i\in\Omega_G, s=2\ldots S \tag{35b}$$

$$x^{re}_{i,s}\in\{0,1\}\quad\forall i\in\Omega_G, s=1\ldots S \tag{35c}$$

The product $V^{re}_{i}I^{re}_{Gi}$ is approximated by using the middle point of the first interval for the discretization of V^{re}_{i} multiplied by I^{re}_{Gi}, plus successive corrections $(C^{a}_{i,s})$ that depend on $\overline{\zeta}^{re}$, I^{re}_{Gi} and $x^{re}_{i,s}$, according to (36).

$$\widetilde{V}^{re}_{i}\widetilde{I}^{re}_{i}=(\underline{V}\cos\beta+\frac{\overline{\zeta}^{re}}{2})I^{re}_{Gi}+\sum_{s=1}^{S}C^{a}_{i,s}\quad\forall i\in\Omega_G \tag{36a}$$

$$0\le\overline{\zeta}^{re}I^{re}_{Gi}-C^{a}_{i,s}\le\overline{\zeta}^{re}\frac{\overline{P}_{Gi}}{\underline{V}}(1-x^{re}_{i,s})\quad\forall i\in\Omega_G, s=1\ldots S \tag{36b}$$

$$0\le C^{a}_{i,s}\le\overline{\zeta}^{re}\frac{\overline{P}_{Gi}}{\underline{V}}x^{re}_{i,s}\quad\forall i\in\Omega_G, s=1\ldots S \tag{36c}$$

Constraint (36a) is a linear approximation of the product of V^{re}_{i} and I^{re}_{Gi}. Constraints (36b) and (36c) define the values of $C^{a}_{i,s}$, $\forall i\in\Omega_G, s=1\ldots S$. If $x^{re}_{i,s}=0$, then $C^{a}_{i,s}=0$ and $I^{re}_{Gi}\le\overline{P}_{Gi}/\underline{V}$; otherwise $C^{a}_{i,s}=\overline{\zeta}^{re}I^{re}_{Gi}$ and $C^{a}_{i,s}\le\overline{\zeta}^{re}\overline{P}_{Gi}/\underline{V}$, where $\overline{\zeta}^{re}\overline{P}_{Gi}/\underline{V}$ provides a sufficient degree of freedom to $C^{a}_{i,s}$.

Using a similar formulation, the product $V^{re}_{i}I^{im}_{Gi}$ in (31) is approximated by using the middle point of the first interval for the discretization of V^{re}_{i} multiplied by I^{im}_{Gi}, plus successive corrections $(C^{b}_{i,s})$ that depend on $\overline{\zeta}^{re}$, I^{im}_{Gi} and $x^{re}_{i,s}$, according to (37).

$$\widetilde{V}^{re}_{i}\widetilde{I}^{im}_{i}=(\underline{V}\cos\beta+\frac{\overline{\zeta}^{re}}{2})I^{im}_{Gi}+\sum_{s=1}^{S}C^{b}_{i,s}\quad\forall i\in\Omega_G \tag{37a}$$

$$0\le\overline{\zeta}^{re}I^{im}_{Gi}-C^{b}_{i,s}\le\overline{\zeta}^{re}\frac{\overline{P}_{Gi}}{\underline{V}}(1-x^{re}_{i,s})\quad\forall i\in\Omega_G, s=1\ldots S \tag{37b}$$

$$0\le C^{b}_{i,s}\le\overline{\zeta}^{re}\frac{\overline{P}_{Gi}}{\underline{V}}x^{re}_{i,s}\quad\forall i\in\Omega_G, s=1\ldots S \tag{37c}$$

The term $V^{im}_{i}I^{im}_{Gi}$ in (30) is linearized by discretization of V^{im}_{i} using the binary variables $x^{im}_{i,s}\ \forall s=1\ldots S$, where $x^{im}_{i,s}=1$ if V^{im}_{i} is greater than $-\overline{V}\sin\beta+s\overline{\zeta}^{im}$. This condition is modeled in (38) showing how the variables $x^{im}_{i,s}$ are calculated. The constant $\overline{\zeta}^{im}$ is calculated as $2\overline{V}\sin\beta/(S+1)$.

$$-\overline{V}\sin\beta+\overline{\zeta}^{im}\sum_{s=1}^{S}x^{im}_{i,s}\le V^{im}_{i}\le-\overline{V}\sin\beta+\overline{\zeta}^{im}\left(1+\sum_{s=1}^{S}x^{im}_{i,s}\right)$$
$$\forall i\in\Omega_G \tag{38a}$$

$$x^{im}_{i,s}\le x^{im}_{i,s-1}\quad\forall i\in\Omega_G, s=2\ldots S \tag{38b}$$

$$x^{im}_{i,s}\in\{0,1\}\quad\forall i\in\Omega_G, s=1\ldots S \tag{38c}$$

The product $V^{im}_{i}I^{im}_{Gi}$ is approximated by using the middle point of the first interval for the discretization of V^{im}_{i} multiplied by I^{im}_{Gi}, plus successive corrections $(C^{c}_{i,s})$ that depend on $\overline{\zeta}^{im}$, I^{im}_{Gi} and $x^{im}_{i,s}$, according to (39).

$$\widetilde{V}^{im}_{i}\widetilde{I}^{im}_{i}=(-\overline{V}\sin\beta+\frac{\overline{\zeta}^{im}}{2})I^{im}_{Gi}+\sum_{s=1}^{S}C^{c}_{i,s}\quad\forall i\in\Omega_G \tag{39a}$$

$$0\le\overline{\zeta}^{im}I^{im}_{Gi}-C^{c}_{i,s}\le\overline{\zeta}^{im}\frac{\overline{P}_{Gi}}{\underline{V}}(1-x^{im}_{i,s})\quad\forall i\in\Omega_G, s=1\ldots S \tag{39b}$$

$$0\le C^{c}_{i,s}\le\overline{\zeta}^{im}\frac{\overline{P}_{Gi}}{\underline{V}}x^{im}_{i,s}\quad\forall i\in\Omega_G, s=1\ldots S \tag{39c}$$

The product $V^{im}_{i}I^{re}_{Gi}$ in (31) is approximated by using the middle point of the first interval for the discretization of V^{im}_{i} multiplied by I^{re}_{Gi}, plus successive corrections $(C^{d}_{i,s})$ that depend on $\overline{\zeta}^{im}$, I^{re}_{Gi} and $x^{im}_{i,s}$, according to (40).

$$\widetilde{V}^{im}_{i}\widetilde{I}^{re}_{i}=(-\overline{V}\sin\beta+\frac{\overline{\zeta}^{im}}{2})I^{re}_{Gi}+\sum_{s=1}^{S}C^{d}_{i,s}\quad\forall i\in\Omega_G \tag{40a}$$

$$0\le\overline{\zeta}^{im}I^{re}_{Gi}-C^{d}_{i,s}\le\overline{\zeta}^{im}\frac{\overline{P}_{Gi}}{\underline{V}}(1-x^{im}_{i,s})\quad\forall i\in\Omega_G, s=1\ldots S \tag{40b}$$

$$0\le C^{d}_{i,s}\le\overline{\zeta}^{im}\frac{\overline{P}_{Gi}}{\underline{V}}x^{im}_{i,s}\quad\forall i\in\Omega_G, s=1\ldots S \tag{40c}$$

Using the approximations given by (35)–(40), the active and reactive power supplied by the distributed generator at node i represented by (30) and (31) are linearized as shown in (41) and (42).

$$P_{Gi}=\widetilde{V}^{re}_{i}\widetilde{I}^{re}_{i}+\widetilde{V}^{im}_{i}\widetilde{I}^{im}_{i}\quad\forall i\in\Omega_G \tag{41}$$

$$Q_{Gi}=-\widetilde{V}^{re}_{i}\widetilde{I}^{im}_{i}+\widetilde{V}^{im}_{i}\widetilde{I}^{re}_{i}\quad\forall i\in\Omega_G \tag{42}$$

So, the RDS problem considering distributed generation in the EDS is modeled as a mixed-integer linear programming problem through (2)–(5), (10)–(19), (21)–(29) and (32)–(42).

5. Tests and results

The proposed mathematical model for the RDS problem was tested using one test system of 69-nodes [26] and two real test systems of 136 [14] and 417-nodes [27]. The model was implemented in AMPL language [28], while the mixed-integer linear programming problems were solved through the commercial solver CPLEX [29] (called with default options) using a workstation with an Intel *i*7 860 processor.

Table 1
Summary of initial operating condition for the test systems.

System	Active power losses (kW)	Node: $min\{V_i\}$ (pu)	$max\{I_{ij}\}$ (A)
69-nodes	69.78	66: 0.912611	118.49
69-nodes + DG	19.12	28: 0.973158	63.80
136-nodes	320.36	116: 0.930652	143.54
136-nodes + DG	274.80	116: 0.930652	143.54
417-nodes	685.89	138: 0.945390	313.79
417-nodes + DG	392.70	138: 0.945390	313.79

Table 2
Summary of initial operating condition for the test systems with distributed generation.

System	Node	$P_{Gi}(kW)$	Q_{Gi} (kVAr)	pf_{Gi}
69-nodes + DG	60	690.8	227.0	0.950 ↑
136-nodes + DG	55	2005.2	659.1	0.950 ↑
	96	1142.2	375.9	0.950 ↑
417-nodes + DG	50	1799.3	591.4	0.964 ↑
	157	3625.7	1000.0	0.950 ↑
	235	1948.3	640.4	0.950 ↑
	281	2593.4	852.4	0.950 ↑
	300	1629.5	535.6	0.950 ↑
	362	3054.2	1000.0	0.950 ↑

Table 3
Characteristics of mathematical model for the test systems.

System	Constrains	Continuous variables	Binary variables
69-nodes	1530	4543	120
69-nodes + DG	1895	4667	160
136-nodes	3152	9561	266
136-nodes + DG	3882	9809	346
417-nodes	9430	23,276	748
417-nodes + DG	10,540	23,660	868

Three additional tests with the 69, 136 and 417-nodes systems were made (named as 69-nodes + DG, 136-nodes + DG and 417-nodes + DG respectively) with the aim of illustrating the application of the proposed RDS model considering distributed generation. The distributed generators for all systems have $\overline{P}_{Gi}$, $\underline{Q}_{Gi}$ and $\overline{Q}_{Gi}$ as 4000 kW, 0 and 1000 kVAr respectively and the minimum power factor is 0.95 (for both leading and lagging). For all tests, the maximum voltage magnitude and the voltage magnitude of the substation is 1.00 pu. Tables 1 and 2 show the active power losses, minimum voltage magnitude, maximum current flow, the active and reactive generated power and the power factor of the distributed generators in the initial operating condition for all systems.

The 69-nodes system has 74 branches and the parameters R_{re}, R_{im}, K_{im}, $\overline{w}_{ij}^{re}$, $\overline{w}_{ij}^{im}$, $\underline{\theta}$ and $\overline{\theta}$ used are equal to 24, 24, 1, 0.05, 0.04, -1° and 0° respectively. For the first three branches the maximum current flow is 150 A, and 100 A for the other branches. For this test, the minimum voltage magnitude is 0.94 pu. For the 69-nodes + DG test, there is a distributed generator at node 60, S is 20 and the parameters R_{re}, R_{im}, K_{im}, $\overline{w}_{ij}^{re}$, $\overline{w}_{ij}^{im}$, $\underline{\theta}$, $\overline{\theta}$, the maximum current flows in the branches and the minimum voltage magnitude are the same as the 69-nodes test.

The 136-nodes system has 156 branches and the parameters R_{re}, R_{im} and K_{im}, $\overline{w}_{ij}^{re}$, $\overline{w}_{ij}^{im}$, $\underline{\theta}$ and $\overline{\theta}$ used are equal to 24, 24, 1, 0.05, 0.04, -4° and 1°, respectively, with a maximum current flow of 200 A for all branches. For this test, the minimum voltage magnitude is 0.95 pu. For the 136-nodes + DG test, there are distributed generators at nodes 55 and 96, S is 20, $\underline{\theta}$ is -2° and $\overline{\theta}$ is 1°. The parameters R_{re}, R_{im}, K_{im}, $\overline{w}_{ij}^{re}$, $\overline{w}_{ij}^{im}$, the maximum current flows in the branches and the minimum voltage magnitude are the same as the 136-nodes test.

The 417-nodes system has 473 branches and it used R_{re}, R_{im}, K_{im}, $\overline{w}_{ij}^{re}$, $\overline{w}_{ij}^{im}$, $\underline{\theta}$ and $\overline{\theta}$ equal to 24, 12, 0.5, 0.04, 0.02, -2° and 1° respectively; a maximum current flow of 300 A was used for all branches. For this test, the minimum voltage magnitude is 0.95 pu. For the 417-nodes + DG test, there are six distributed generators at nodes 50, 157, 235, 281, 300 and 362, S is 10, $\underline{\theta}$ is -1° and $\overline{\theta}$ is 1°. The parameters R_{re}, R_{im}, K_{im}, $\overline{w}_{ij}^{re}$, $\overline{w}_{ij}^{im}$, the maximum current flow in the branches and the minimum voltage magnitude are the same as the 417-nodes test.

The values of S, R_{re}, R_{im}, K_{im}, $\overline{w}_{ij}^{re}$ and $\overline{w}_{ij}^{im}$ were selected through experimental tests with the aim of achieving good accuracy without compromising the efficiency of MILP problem's solution. The characteristics of mathematical models for the all tests are shown in Table 3. Table 4 shows the active power losses, minimum voltage magnitude and maximum current flow of the obtained solutions for all systems and the respective errors in comparison with the results of a single phase load flow appear between parentheses (in %). Table 5 shows the active and reactive generated power, as well as, the power factor of the distributed generators under the solutions obtained for the 69-nodes + DG, 136-nodes + DG and 417-nodes + DG systems. The respective errors in comparison with the calculation of the variables according to (30) and (31) are shown in parentheses. Finally, the disconnected branches for the tested systems are shown in Table 6.

In the initial operating condition of the 69-node system, the minimum voltage magnitude is below its minimum limit and has active power losses of 69.78 kW. For this test, the proposed method obtained the same solution for the RDS problem than the one presented in [30], with active power losses of 30.09 kW (a reduction of 56.9%) and a minimum voltage magnitude above its minimum limit. The optimal topology is depicted in Fig. 6. In the initial operating condition of the 69-nodes + DG test, the active power losses is 19.12 kW, the minimum voltage magnitude is above its minimum limit and the generator produces active and reactive power within its limits with a leading power factor of 0.95. The proposed method obtained a solution for the RDS problem with active power losses of 14.02 kW (a reduction of 26.7%); with the optimal topology depicted in Fig. 7. The generator produces active and reactive power within its limits with a leading power factor of 0.95 and the minimum voltage magnitude is above its minimum limit.

For the 136-nodes system, the initial operating condition has an active power losses of 320.36 kW and a minimum voltage magnitude below its minimum limit. The proposed method obtained a solution for the RDS problem with active power losses of 280.19 kW (a reduction of 12.5%) which is the best-known solution for this

Table 4
Summary of results for test systems.

System	Active power losses (kW)	Node: $min\{V_i\}$ (pu)	$max\{I_{ij}\}$ (A)
69-nodes	29.98 (−0.36%)	62: 0.945254 (+0.002%)	116.18 (−0.00%)
69-nodes + DG	13.88 (−0.97%)	65: 0.968961 (−0.006%)	75.83 (−0.09%)
136-nodes	279.85 (−0.12%)	105: 0.958921 (+0.001%)	145.61 (+0.02%)
136-nodes + DG	162.20 (−0.35%)	105: 0.966661 (+0.018%)	170.40 (+0.16%)
417-nodes	581.32 (−0.08%)	42: 0.954776 (+0.001%)	280.32 (+0.00%)
417-nodes + DG	266.60 (−0.36%)	48: 0.950523 (+0.016%)	220.93 (+0.00%)

Table 5
Summary of results for the test systems with distributed generation.

System	Node	$P_{Gi}(kW)$	Q_{Gi} (kVAr)	pf_{Gi}
69-nodes + DG	60	510.6 (+0.11%)	167.8 (−0.32%)	0.950 ↑
136-nodes + DG	55	3987.8 (−0.07%)	1000.0 (−0.88%)	0.970 ↑
	96	3493.3 (−0.13%)	1000.0 (−0.22%)	0.961 ↑
417-nodes + DG	50	3213.2 (−0.02%)	1000.0 (−0.51%)	0.954 ↑
	157	2162.3 (+0.00%)	710.7 (−1.00%)	0.950 ↑
	235	2015.1 (+0.08%)	662.3 (−0.09%)	0.950 ↑
	281	3738.8 (−0.13%)	1000.0 (−0.64%)	0.966 ↑
	300	1446.5 (−0.14%)	474.8 (−0.74%)	0.950 ↑
	362	3437.4 (−0.19%)	1000.0 (−0.74%)	0.960 ↑

Table 6
Disconnected branches for the tests systems.

System	Disconnected branches
69-nodes	15, 56, 62, 70, 71
69-nodes + DG	13, 56, 65, 70, 71
136-nodes	7, 35, 51, 90, 96, 106, 118, 126, 135, 137, 138, 141, 142, 144, 145, 146, 147, 148, 150, 151, 155
136-nodes + DG	9, 15, 25, 49, 62, 83, 90, 93, 104, 106, 132, 135, 136, 139, 144, 145, 147, 148, 150, 154, 155
417-nodes	5, 13, 15, 16, 21, 26, 31, 54, 55, 57, 60, 73, 86, 87, 94, 96, 97, 111, 115, 136, 142, 148, 149, 150, 155, 158, 163, 168, 169, 178, 179, 191, 195, 199, 213, 214, 252, 254, 266, 282, 297, 310, 325, 358, 359, 362, 369, 392, 395, 400, 402, 403, 416, 423, 431, 436, 437, 446, 449
417-nodes + DG	2, 4, 5, 6, 13, 15, 16, 21, 29, 31, 34, 43, 57, 60, 86, 96, 97, 99, 116, 119, 126, 136, 143, 148, 150, 158, 163, 165, 168, 175, 183, 188, 194, 214, 217, 228, 250, 252, 267, 278, 294, 297, 325, 330, 362, 369, 384, 388, 395, 400, 402, 416, 419, 423, 431, 436, 445, 446, 462

system, as shown in [14], with a minimum voltage magnitude above its minimum limit. In the initial operating condition of the 136-nodes + DG test the active power losses is 274.80 kW, the minimum voltage magnitude is below its minimum limit and the generators produce active and reactive power within its limits with a leading power factor of 0.95. The proposed method obtained a solution for the RDS problem with active power losses of 162.77 kW (a reduction of 40.8%), with a minimum voltage magnitude above its minimum limit. Note that, the first generator produces active power near its maximum capacity while the second produces active power above 87% their maximum capacity, both generating reactive power reaching their limits. The two generators are operating with leading power factors within their limits.

In the initial operating condition of the 417-node system, the active power losses is 685.89 kW and the minimum voltage magnitude is below its minimum limit. The proposed method found a solution for the RDS problem with active power losses of 581.79 kW (a reduction of 15.2%), and a minimum voltage magnitude above its minimum limit. For the 417-nodes + DG test, the initial operating condition has an active power losses of 392.70 kW and a minimum voltage magnitude below its minimum limit. The distributed generators at nodes 157 and 362 produce active power above 75% their maximum capacities, generating reactive power reaching their limits. The other four distributed generators produce active and reactive power within their limits. All the generators are operating with leading power factors and five operating in their

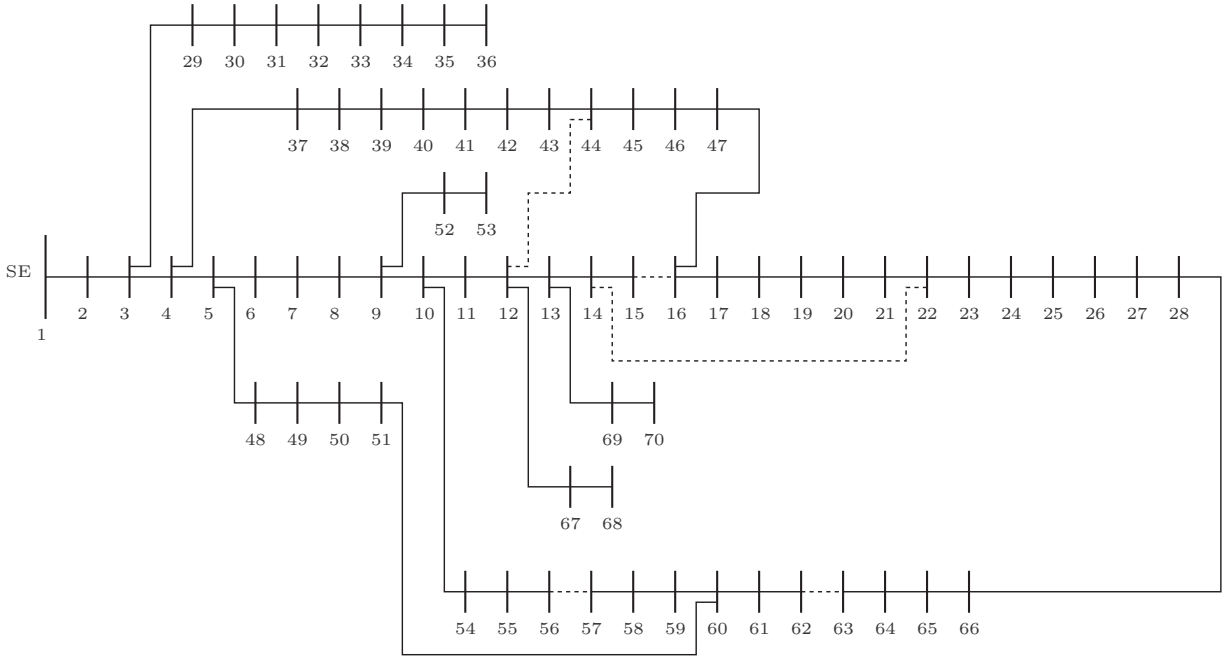

Fig. 6. Optimal topology for the test system of 69-nodes.

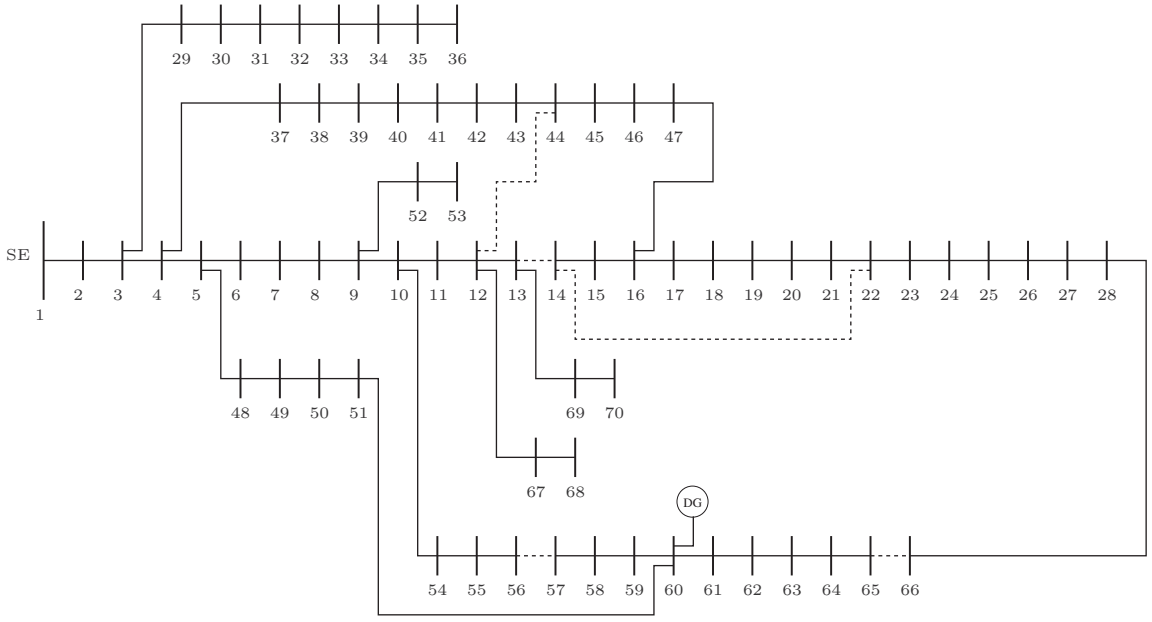

Fig. 7. Optimal topology for the test system of 69-nodes + DG.

minimum limit of 0.95. The proposed method obtained a solution for the RDS problem with active power losses of 267.56 kW (a reduction of 31.9%) with the minimum voltage magnitude above its minimum limit. Note that, distributed generators at nodes 50, 281 and 362 produce active power above 80% of their maximum capacities, generating reactive power reaching their limits. The other three distributed generators at nodes 157, 235 and 300 produce active and reactive power within their limits. All the generators are operating with leading power factors, four operating in their minimum limit of 0.95.

From Tables 4 and 5 it can be observed that the percentage errors of active power losses, minimum voltage magnitude, maximum current flow and generated power are small and less than 1.00%, 0.02%, 0.20% and 1.00% respectively for all systems. Also, the increase of the dimension of the systems does not harm the accuracy of results. From Table 6, the topology found with and without the presence of distributed generation is different for all systems, showing the importance of considering distributed generations in the RDS problem.

6. Conclusion

A mixed-integer linear model for the problem of reconfiguration of electric distribution systems was presented. The use of a MILP formulation has the following benefits: (a) a robust mathematical model that is equivalent to the MINLP model; (b) an efficient computational behavior with exiting MILP solvers; and (c) guarantees convergence to optimality using classical optimization techniques. The proposed model takes into account the presence of distributed generators in the system. Constant power, constant current and constant impedance types demands were modeled using a linear approximation in terms of the real and imaginary parts of the voltage.

It was shown that the phase angles remain within a relatively small and limited range for the typical operating conditions of an EDS. A system of linear equations to calculate the steady-state operation of an EDS was also presented. The results show that the active power losses, voltage magnitude, and current flow magnitudes are calculated with great precision in comparison with the load flow sweep method.

The results obtained show that, for the 69 and 136-nodes systems, the proposed method found the best-known solutions for the RDS problem. Additionally, for the 417-nodes system a good quality solution was found.

Appendix A. Effect of voltage magnitude levels on EDS loads

Eqs. (43) and (44) are second order polynomial equations that represent the effect of voltage magnitude levels on EDS loads.

$$P_{D_i} = P_{0_i} + P_{1_i} V_i + P_{2_i} V_i^2 \quad \forall i \in \Omega_b \tag{43}$$

$$Q_{D_i} = Q_{0_i} + Q_{1_i} V_i + Q_{2_i} V_i^2 \quad \forall i \in \Omega_b \tag{44}$$

where P_{0_i} and Q_{0_i} represent the constant power component at node i, P_{1_i} and Q_{1_i} represent the constant current component at node i, P_{2_i} and Q_{2_i} represent the impedance power component at node i.

Appendix B. Analysis of the phase angle variation in EDS

It is well known that the determination of the state variables of EDS is performed by solving the power flow or load flow problem. These variables are the voltage phasors of the nodes. Taking advantage of the operation features of an EDS, iterative specialized algorithms to solve the load flow problem were developed, as shown in [20,24,25].

Of the main features of the EDS, it is important to note: (a) the radial topology of the feeders; (b) lines of very different lengths; (c) a high R/X ratio when compared with typical values found in transmission systems; (d) loads are encouraged to correct its load power factor for standard ranges; and (e) the need to ensure that the voltage magnitudes are within allowable ranges.

Taking into account the last three features above, it can be shown that the phase angles in all EDS nodes are small. Consider a load with an active power P_{Dj} and a reactive power Q_{Dj} at node j, fed by a branch between nodes i and j with impedance $R_{ij} + jX_{ij}$. The voltage magnitude V_j and phase angle θ_j at node j can be calculated according to (45) and (46) (see [25]).

$$V_j^4 + [2(P_{Dj}R_{ij} + Q_{Dj}X_{ij}) - V_i^2]V_j^2 + (P_{Dj}^2 + Q_{Dj}^2)(R_{ij}^2 + X_{ij}^2) = 0 \tag{45}$$

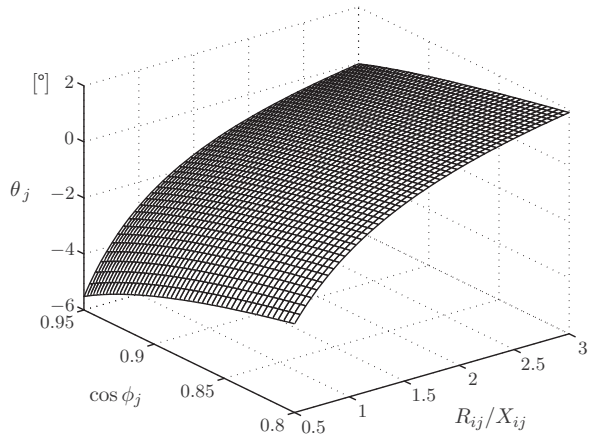

Fig. 8. Variation of the phase angle θ_j.

$$\sin(\theta_i - \theta_j) = \frac{P_{Dj}X_{ij} - Q_{Dj}R_{ij}}{V_i V_j} \tag{46}$$

Eqs. (45) and (46) can be written in terms of the factor $P_{Dj}X_{ij}$, the R_{ij}/X_{ij} ratio, and the angle ϕ_j associated with the load power factor at node j ($\tan\phi_j = Q_{Dj}/P_{Dj}$), as shown in (47) and (48).

$$(P_{Dj}X_{ij})^2\left(1+\left(\frac{R_{ij}}{X_{ij}}\right)^2\right)\sec^2(\phi_j) + 2V_j^2(P_{Dj}X_{ij})\left(\frac{R_{ij}}{X_{ij}} + \tan(\phi_j)\right) + (V_j^4 - V_i^2V_j^2) = 0 \tag{47}$$

$$\theta_j = \theta_i - \arcsin\left((P_{Dj}X_{ij})\frac{1-(R_{ij}/X_{ij})\tan\phi_j}{V_iV_j}\right) \tag{48}$$

Note that θ_j is proportional to the loading and electrical parameters of the branch, represented by the $P_{Dj}X_{ij}$ factor. If the voltage magnitudes must be within the range $[\underline{V}, \overline{V}]$ pu, defined by the system operator, we can assume the worst case of voltage regulation to be $V_i = \overline{V}$ pu and $V_j = \underline{V}$ pu.

Thus, for given values of the R_{ij}/X_{ij} ratio and load power factor, $\cos\phi_j$, it is possible to calculate the phase angle at node j. Fig. 8 shows the behavior of the phase angle θ_j, considering $\theta_i = 0^\circ$, $\overline{V} = 1.0$ pu, $\underline{V} = 0.9$ pu, R_{ij}/X_{ij} ratio varying in the range [0.50, 3.00] and load power factor varying in the range [0.80, 0.95]. For these typical operating conditions of the EDS, the phase angle remains in the range $[-5.52, 1.90]^\circ$.

So, we can conclude that the following applies to θ_j: (a) it is directly proportional to the R_{ij}/X_{ij} ratio; (b) it is inversely proportional to the load power factor; and (c) it remains within a relatively small and limited range for typical operating conditions of an EDS.

Appendix C. Notation

The notation used throughout this paper is reproduced below for quick reference.

Sets

Ω_b	sets of nodes
Ω_l	sets of branches
Ω_g	sets of distributed generators

Constants

$\underline{V}$	minimum voltage magnitude (kV)
$\overline{V}$	maximum voltage magnitude (kV)
$\overline{I}_{ij}$	maximum current flow of branch ij (A)
R_{ij}	resistance of branch ij (Ω)
X_{ij}	reactance of branch ij (Ω)
a_i, b_i, c_i	coefficients used in the linearization of the real part of current demand at node i
d_i, e_i, f_i	coefficients used in the linearization of the imaginary part of current demand at node i
$\overline{\theta}$	maximum phase angle
$\underline{\theta}$	minimum phase angle
$\overline{\beta}$	maximum absolute value of phase angle
$\overline{P}_{Gi}$	maximum active power of distributed generator at node i
$\underline{Q}^{Gi}$	minimum reactive power of distributed generator at node i
$\overline{Q}_{Gi}$	maximum reactive power of distributed generator at node i
$pf_{Gi}\uparrow$	minimum leading power factor of distributed generator at node i
$pf_{Gi}\downarrow$	minimum lagging power factor of distributed generator at node i
$\overline{w}_{ij}^{re}$	upper bound for w_{ij}^{re}
$\overline{w}_{ij}^{im}$	upper bound for w_{ij}^{im}
R_{re}	number of blocks of the piecewise linearization for the real part of the current of branch ij
R_{im}	number of blocks of the piecewise linearization for the imaginary part of the current of branch ij
$\overline{\Delta}_{ij}^{re}$	discretization step for the real part of the current of branch ij
$\overline{\Delta}_{ij}^{im}$	discretization step for the imaginary part of the current of branch ij
$m_{ij,r}^{re}$	slope of the rth block of the piecewise linearization for the real part of the current of branch ij
$m_{ij,r}^{im}$	slope of the rth block of the piecewise linearization for the imaginary part of the current of branch ij
$\overline{\zeta}^{re}$	upper bound of each block of the discretization of the real component of the voltage
$\overline{\zeta}^{im}$	upper bound of each block of the discretization of the imaginary component of the voltage
S	number of discretizations of the voltage
K_{im}	ratio used in the piecewise linearization for the imaginary part of the current of branch ij

Functions

P_{Di}	active power demand at node i that varies according to the voltage magnitude (kW)
Q_{Di}	reactive power demand at node i that varies according to the voltage magnitude (kVAr)

Variables

V_i	voltage magnitude at node i
θ_i	phase angle of the voltage at node i
V_i^{re}	real part of voltage at node i
V_i^{im}	imaginary part of voltage at node i
P_{Gi}	active power generated at node i
Q_{Gi}	reactive power generated at node i
I_{ij}^{re+}	real part of current flow of branch ij in the forward direction
I_{ij}^{re-}	real part of current flow of branch ij in the backward direction
I_{ij}^{im+}	imaginary part of current flow of branch ij in the forward direction
I_{ij}^{im-}	imaginary part of current flow of branch ij in the backward direction
I_{ij}^{sqr}	square current flow magnitude of branch ij
I_{Di}^{re}	real part of current demand at node i

I_{Di}^{im} imaginary part of current demand at node i
I_{Gi}^{re} real part of current generated at node i
I_{Gi}^{im} imaginary part of current generated at node i
w_{ij}^{re} variable used in the calculation of the real component of the drop voltage for branch ij
w_{ij}^{im} variable used in the calculation of the imaginary component of the drop voltage for branch ij
$\widetilde{V}_i^{re}\widetilde{I}_i^{re}$ approximation of the product $V_i^{re}I_{Gi}^{re}$
$\widetilde{V}_i^{re}\widetilde{I}_i^{im}$ approximation of the product $V_i^{re}I_{Gi}^{im}$
$\widetilde{V}_i^{im}\widetilde{I}_i^{im}$ approximation of the product $V_i^{im}I_{Gi}^{im}$
$\widetilde{V}_i^{im}\widetilde{I}_i^{re}$ approximation of the product $V_i^{im}I_{Gi}^{re}$
$\Delta_{ij,r}^{re}$ value of the rth block of $I_{ij}^{re+} + I_{ij}^{re-}$
$\Delta_{ij,r}^{im}$ value of the rth block of $I_{ij}^{im+} + I_{ij}^{im-}$
$C_{i,s}^{a}$ variable used in the approximation of $V_i^{re}I_{Gi}^{re}$
$C_{i,s}^{b}$ variable used in the approximation of $V_i^{re}I_{Gi}^{im}$
$C_{i,s}^{c}$ variable used in the approximation of $V_i^{im}I_{Gi}^{im}$
$C_{i,s}^{d}$ variable used in the approximation of $V_i^{im}I_{Gi}^{re}$
$x_{i,s}^{re}$ binary variable used in the discretization of the real component of the voltage
$x_{i,s}^{im}$ binary variable used in the discretization of the imaginary component of the voltage
y_{ij}^{+} binary variable used in the reconfiguration of the branch ij in the forward direction
y_{ij}^{-} binary variable used in the reconfiguration of the branch ij in the backward direction

References

[1] A. Merlin, G. Back, Search for minimum-loss operational spanning tree configuration for an urban power distribution system, in: Proc. of the 5th Power System Conf., Cambridge, 1975, pp. 1–18.
[2] T.P. Wagner, A.Y. Chikhani, R. Hackam, Feeder reconfiguration for loss reduction: an application of distribution automation, IEEE Transactions on Power Delivery 6 (October (4)) (1991) 1922–1933.
[3] A. Abur, A modified linear programming method for distribution system reconfiguration, International Journal of Electrical Power & Energy Systems 18 (May (7)) (1996) 469–474.
[4] G. Celli, M. Loddo, F. Pilo, A. Abur, On-line network reconfiguration for loss reduction in distribution networks with distributed generation, in: 18th Int. Conf. on Electricity Dist., vol. 18, no. 7, June, 2005, 2005, pp. 6–9.
[5] E.R. Ramos, A.G. Expósito, J.R. Santos, F.L. Iborra, Path-based distribution network modeling: application to reconfiguration for loss reduction, IEEE Transactions on Power Systems 20 (May (2)) (2005) 556–564.
[6] E. Romero-Ramos, J. Riquelme-Santos, J. Reyes, A simpler and exact mathematical model for the computation of the minimal power losses tree, International Journal of Electric Power Systems Research 80 (May) (2010) 562–571.
[7] R.A. Jabr, R. Singh, B.C. Pal, Minimum loss network reconfiguration using mixed-integer convex programming, IEEE Transactions on Power Systems 27 (May (2)) (2012) 1106–1115.
[8] Y.J. Jeon, J.C. Kim, J.O. Kim, J.R. Shin, K.Y. Lee, An efficient simulated annealing algorithm for network reconfiguration in large-scale distribution systems, IEEE Transactions on Power Delivery 17 (October (4)) (2002) 1070–1078.
[9] V. Parada, J.A. Ferland, M. Arias, K. Daniels, Optimization of electric distribution feeders using simulated annealing, IEEE Transactions on Power Delivery 19 (July) (2004) 1135–1141.
[10] C.F. Chang, Reconfiguration and capacitor placement for loss reduction of distribution systems by ant colony search algorithm, IEEE Transactions on Power Systems 23 (November (4)) (2008) 1747–1755.
[11] S. Ching-Tzong, C. Chung-Fu, C. Ji-Pyng, Distribution network reconfiguration for loss reduction by ant colony search algorithm, International Journal of Electric Power Systems Research 75 (2/3) (2005) 190–199.
[12] A.Y. Abdelaziz, F.M. Mohammed, S.F. Mekhamer, M.A.L. Badr, Distribution systems reconfiguration using a modified particle swarm optimization algorithm, International Journal of Electric Power Systems Research 79 (11) (2009) 1521–1530.
[13] J. Mendoza, R. Lopez, D. Morales, E. Lopez, P. Dessante, R. Moraga, Minimal loss reconfiguration using genetic algorithms with restricted population and addressed operators: real application, IEEE Transactions on Power Systems 21 (May (2)) (2006) 948–954.
[14] E. Carreño, R. Romero, A. Padilha-Feltrin, An efficient codification to solve distribution network reconfiguration for loss reduction problem, IEEE Transactions on Power Systems 23 (November (4)) (2008) 1542–1551.
[15] K. Prasad, R. Ranjan, N.C. Sahoo, A. Chaturvedi, Optimal reconfiguration of radial distribution systems using a fuzzy mutated genetic algorithm, IEEE Transactions on Power Delivery 20 (April (2)) (2005) 1211–1213.
[16] D. Zhang, Z. Fu, L. Zhang, An improved TS algorithm for loss-minimum reconfiguration in large-scale distribution systems, International Journal of Electric Power Systems Research 77 (5/6) (2007) 685–694.
[17] A.Y. Abdelaziz, F.M. Mohamed, S.F. Mekhamer, M.A.L. Badr, Distribution system reconfiguration using a modified tabu search algorithm, International Journal of Electric Power Systems Research 80 (2010) 943–953.
[18] F. Gomes, S. Carneiro, J.L.R. Pereira, M. Vinagre, P. Garcia, L. Araujo, A new heuristic reconfiguration algorithm for large distribution systems, IEEE Transactions on Power Systems 20 (August (3)) (2005) 1373–1378.
[19] M.E. Baran, F.F. Wu, Network reconfiguration in distribution systems for loss reduction and load balancing, IEEE Transactions on Power Delivery 4 (April (2)) (1989) 1401–1407.
[20] S.K. Goswami, S.K. Basu, A new algorithm for the reconfiguration of distribution feeders for loss minimization, IEEE Transactions on Power Delivery 7 (July (3)) (1992) 1484–1491.
[21] J.A. Martin, A.J. Gil, A new heuristic approach for distribution systems loss reduction, International Journal of Electric Power Systems Research 78 (November (11)) (2008) 1953–1958.
[22] A.R. Abul'Wafa, A new heuristic approach for optimal reconfiguration in distribution systems, International Journal of Electric Power Systems Research 81 (February (2)) (2011) 282–289.
[23] M. Lavorato, J. Franco, M.J. Rider, R. Romero, Imposing radiality constraints in distribution system optimization problems, IEEE Transactions on Power Systems 27 (February (1)) (2012) 172–180.
[24] D. Shirmohammadi, H.W. Hong, A. Semlyen, G.X. Luo, A compensation-based power flow method for weakly meshed distribution and transmission networks, IEEE Transactions on Power Systems 3 (May (2)) (1988) 753–762.
[25] R. Cespedes, New method for the analysis of distribution networks, IEEE Transactions on Power Delivery 5 (January (1)) (1990) 391–396.
[26] H.D. Chiang, R.M. Jean-Jameau, Optimal network reconfiguration in distribution systems, part 2. Solution algorithms and numerical results, IEEE Transactions on Power Delivery 5 (July (3)) (1990) 1568–1574.
[27] I.J. Ramírez-Rosado, J.L. Bernal-Augustín, Genetic algorithms applied to the design of large power distribution systems, IEEE Transactions on Power Systems 13 (May (2)) (1998) 696–703.
[28] R. Fourer, D.M. Gay, B.W. Kernighan, AMPL: A Modeling Language for Mathematical Programming, 2nd ed., Brooks/Cole-Thomson Learning, Pacific Grove, CA, 2003.
[29] CPLEX Optimization Subroutine Library Guide and Reference, Version 12.2, CPLEX Division, ILOG Inc., Incline Village, NV, USA, 2010.
[30] G. Raju, P.R. Bijwe, An efficient algorithm for minimum loss reconfiguration of distribution system based on sensitivity and heuristics, IEEE Transactions on Power Systems 23 (August (3)) (2008) 1280–1287.